International Journal of Fracture (2005) 132:349–368
DOI 10.1007/s10704-005-1890-x

Thermal fracture interference: a two-dimensional boundary element approach

G.I. GIANNOPOULOS and N.K. ANIFANTIS*
Machine Design Laboratory, Mechanical and Aeronautics Engineering Department, University of Patras, Greece
**Author for correspondence. (E-mail: nanif@mech.upatras.gr, Phone: +30-2610-997-197, Fax: +30-2610-997-207)*

Received 17 May 2004; accepted in revised form 8 February 2005

Abstract. Thermal loading of fractured structures is associated with the development of differential deformations along crack surfaces which result in the closure of the crack. Inherent non-linearities demand application of numerical procedures to resolve this problem. In this paper, a boundary element procedure is formulated to treat crack surface interference imposed under thermal steady-state or transient loadings. An iterative-incremental procedure is developed to deal with the non-linearity produced by the frictional contact of the crack surfaces. The open, adhesion and slip contact conditions are modeled through the utilization of the multi-domain technique. Two approaches are followed regarding the thermal boundary contact conditions along the crack region. In the first, crack surfaces are assumed to be thermally insulated. This assumption simplifies the formulation significantly. In the second, the crack surfaces are assumed to provide perfect thermal contact. Thermal stress intensity factors are evaluated from traction nodal results that adopt singular elements in the crack tip region. Numerical examples are illustrated, discussed and compared with analytical solutions, where possible. Fracture characteristics are predicted in terms of the involved parameters. As a general conclusion, peak values of thermal stress intensity factors depend on the friction conditions existing between crack faces.

Key words: Boundary element analysis, crack closure, frictional contact analysis, incremental procedure, stress intensity factor, thermal shock.

1. Introduction

The processing of modern material components usually involves heat treatment procedures. During the operating cycles, these components undergo complex mechanical and thermal conditions. The complicated geometry configurations combined with the developed steep temperature gradients, enforce failures which reduce the reliability standards and substantially increase the manufacturing or maintenance costs. As there is a demand for better reliability standards, the development of preventive design methodologies that can be applicable under extreme loading conditions in the presence of cracks, has become more and more essential. Despite the fact that the role of mechanical loading in fracture has been investigated, it is of fundamental importance to understand how transient or cyclic thermal conditions affect crack growth and fatigue failure. When this kind of dynamic load is dominated, cracks tend to open and close regularly. Because of this, a more complicated modeling is

demanded, as the open crack assumption is violated. During the contact phenomenon, the crack surfaces come into contact and form an interface on which contact pressure and friction forces interact in the normal and tangential direction, respectively. The interference of the deformations of the crack faces is commonly referred in the literature as crack closure. Contact fracture mechanics typically involves partial contact of the two faces of the crack under applied thermal load. Despite the significance of crack closure and its effect on the crack growth rates, its characterization under time-dependent thermal loading has not been resolved because it involves substantial computational effort.

Contact problems are non-linear because the contact surfaces are not known *a priori* and due to the load-dependency of the contact conditions along the contact area. When the contact area is located on a crack (crack closure phenomenon), then the difficulty in approaching these problems is increased due to the presence of field singularities near the crack tip. Under crack contact conditions, the near crack tip displacements and stresses keep their essential singular behavior, despite the imposed contact constraints. However, because of the non-linearity of the contact phenomenon, an accurate analytical solution is not possible.

Among general computational techniques, which have been developed to treat crack contact problems, it must be acknowledged that the finite element method (FEM) has hitherto been the most successful (McClung and Sehitoglou, 1989; Kokini and Reynolds, 1991; Anifantis, 2001). However, the requirement for dense mesh refinement in the neighborhood of the crack arises computational deficiencies. The boundary element method (BEM) has been successfully applied to general elastic frictional contact problems (Karami, 1983; Man et al., 1993) and has also been used as an alternative potential tool in analyzing crack contact problems involving pure mechanical loads (Karami and Fenner, 1986; Zang and Gudmundson, 1990; Liu and Tan, 1992). Nevertheless, there is a lack of equivalent material for steady-state and transient thermoelastic fracture problems. The thermal shock fracture problem related with surface cooling – causing crack opening – was solved in detail by Nied (1983) through integral equation techniques. Nied (1987) as well as Rizk and El-Fattah (1993) attempted to quantify the severity of surface heating induced crack closure in a cracked plate of finite thickness. However, in this work only symmetrical cracks under symmetrical loadings were investigated and thus the effect of friction was not examined.

In thermal fracture mechanics analysis, the determination of the stress intensity factor (SIF) is always a major consideration and it has to be evaluated. One approach is to utilize singular elements. Among those, the quarter-point element (QPE) has been significantly popular because of its accuracy and simplicity (Martinez and Dominguez, 1984; Katsareas and Anifantis, 1996). Karami and Fenner (1986) investigated crack closure problems of strips with edge or inclined central cracks by utilizing the standard quadratic isoparametric multi-domain BEM formulation and quarter-point crack tip elements to represent the singularity of the near-tip displacement fields. Selvadurai and Au (1988) used the traction singular crack tip element even in the case of a closed crack tip.

In this study, an iterative-incremental procedure based on the multi-domain BEM has been developed for the analysis of two-dimensional frictional crack closure under thermal loading. The so-called multi-domain technique permits subdivision of the

problem domain into sub-regions. The crack surfaces are modeled as separate boundary surfaces, on which appropriate constraints, involving traction-free, adhesion or slip contact conditions, are imposed. In order to model the thermal crack closure, two different formulations are utilized. Firstly, the crack is assumed fully adiabatic and secondly, perfect thermal conduction is assumed between the crack faces along the contact zone. The common isoparametric quadratic elements in conjunction with special crack tip elements are utilized. The results that are presented here correspond to a variety of crack orientations, friction and heating conditions.

2. BEM formulation for 2D thermoelasticity

The boundary integral equations describing two-dimensional thermoelastic problems are well-known. In order to keep the reader aware of the method, these equations are described briefly in the following.

2.1. Steady-state thermoelasticity

Considering a two-dimensional isotropic and homogenous solid, free of heat and body forces, defined on domain Ω of boundary Γ, the boundary integral equations governing the steady-state thermoelastic equilibrium can be written in the following form (Brebbia et al., 1984; Balas et al., 1989; Raveendra and Banerjee, 1992):

$$c(\xi)\theta(\xi) + \int_\Gamma \theta(\boldsymbol{x}) Q(\boldsymbol{x}, \xi) \mathrm{d}\Gamma(\boldsymbol{x}) = \int_\Gamma q(\boldsymbol{x}) \Theta(\boldsymbol{x}, \xi) \mathrm{d}\Gamma(\boldsymbol{x}) \tag{1}$$

$$c_{ij}(\xi) u_j(\xi) + \int_\Gamma u_j(x) T_{ij}(x, \xi) \mathrm{d}\Gamma(x) = \int_\Gamma t_j(x) U_{ij}(x, \xi) \mathrm{d}\Gamma(x) + \int_\Gamma [\theta(x) \overline{Q}_i(x, \xi) - q(x) \overline{\Theta}_i(x, \xi)] \mathrm{d}\Gamma(x), \tag{2}$$

where the indices i, j assign the global Cartesian directions along the axis x_i, x_j, respectively, with $i, j = 1, 2$; θ, q are the temperature and the heat flux; u_j, t_j denote components of the boundary displacement and traction vectors, respectively. The vectors $\boldsymbol{x}$ and ξ are the source and field points; c, c_{ij} are functions of the local geometry at ξ. The functions $Q(\boldsymbol{x}, \xi)$, $\Theta(\boldsymbol{x}, \xi)$, $T_{ij}(\boldsymbol{x}, \xi)$, $U_{ij}(\boldsymbol{x}, \xi)$, $\overline{\Theta}_i(\boldsymbol{x}, \xi)$, $\overline{Q}_i(\boldsymbol{x}, \xi)$ are the fundamental solutions for two-dimensional stationary thermoelasticity. Details for the derivation and the form of these functions may be found elsewhere (Brebbia et al., 1984; Balas et al., 1989; Raveendra and Banerjee, 1992).

According to the BEM procedures, the boundary of the body is discretized into a number of standard quadratic isoparametric elements. Over each element the variations of the geometry, displacements and tractions are described in terms of nodal values, by the corresponding shape functions (Brebbia et al., 1984). Note that in the problems considered in this work, standard isoparametric elements are used everywhere in the boundary except for the crack tips where special elements, which will be described later on, are utilized.

After discretizing Equations (1) and (2) and assembling, two systems of equations are produced that in the usual terminology of BEM, can be expressed in the

following form:

$$[\boldsymbol{Q}]\{\boldsymbol{\theta}\}=[\boldsymbol{\Theta}]\{\boldsymbol{q}\}, \tag{3}$$

$$[\boldsymbol{T}]\{\boldsymbol{u}\}=[\boldsymbol{U}]\{\boldsymbol{t}\}+\{\boldsymbol{B}\}. \tag{4}$$

In last equations, matrixes $[\boldsymbol{Q}]$, $[\boldsymbol{\Theta}]$, $[\boldsymbol{T}]$ and $[\boldsymbol{U}]$ contain coefficients which represent integrations of Q_i, Θ_i, T_{ij} and U_{ij} over the elements, respectively. The singular diagonal terms of matrixes $[\boldsymbol{Q}]$ and $[\boldsymbol{T}]$ containing the function $c(\xi)$ and $c_{ij}(\xi)$, respectively, are obtained through the well-known rigid body technique (Brebbia et al., 1984). The last term of Equation (4) is defined as:

$$\{\boldsymbol{B}\}=[\overline{\boldsymbol{Q}}]\{\boldsymbol{\theta}\}-[\overline{\boldsymbol{\Theta}}]\{\boldsymbol{q}\}, \tag{5}$$

where matrixes $[\overline{\boldsymbol{Q}}]$ and $[\overline{\boldsymbol{\Theta}}]$ contain coefficients which represent integrations of $\overline{Q}_i$ and $\overline{\Theta}_i$ over the elements, respectively. Finally θ and q are the temperatures and heat fluxes derived from Equation (3).

2.2. Quasistatic thermoelasticity

The boundary integral equations governing the two-dimensional quasistatic problem of a thermoelastic solid, defined on domain Ω of boundary Γ in the absence of internal sources, are (Brebbia et al., 1984; Balas et al., 1989; Raveendra and Banerjee, 1992):

$$\begin{aligned} c(\xi)\theta(\xi,t_{\mathrm{F}})+\int_{t_0}^{t_{\mathrm{F}}}\int_{\Gamma}\theta(\boldsymbol{x},t)Q(\boldsymbol{x},\xi,t_{\mathrm{F}},t)\,\mathrm{d}\Gamma(\boldsymbol{x})\,\mathrm{d}t-\int_{\Omega}\theta_0(\boldsymbol{x})Q(\boldsymbol{x},\xi,t_{\mathrm{F}},t_0)\,\mathrm{d}\Omega(\boldsymbol{x})\\ =\int_{t_0}^{t_{\mathrm{F}}}\int_{\Gamma}q(\boldsymbol{x},t)\Theta(\boldsymbol{x},\xi,t_{\mathrm{F}},t)\,\mathrm{d}\Gamma(\boldsymbol{x})\,\mathrm{d}t, \end{aligned} \tag{6}$$

$$\begin{aligned} c_{ij}(\xi)u_j(\xi,t_{\mathrm{F}})+\int_{\Gamma}u_j(\boldsymbol{x},t_{\mathrm{F}})T_{ij}(\boldsymbol{x},\xi)\,\mathrm{d}\Gamma(\boldsymbol{x})\\ =\int_{\Gamma}t_j(\boldsymbol{x},t_{\mathrm{F}})U_{ij}(\boldsymbol{x},\xi)\,\mathrm{d}\Gamma(\boldsymbol{x})+\int_{t_0}^{t_{\mathrm{F}}}\int_{\Gamma}[\theta(\boldsymbol{x},t)\overline{Q}_i(\boldsymbol{x},\xi,t_{\mathrm{F}},t)\\ -q(\boldsymbol{x},t)\overline{\Theta}_i(\boldsymbol{x},\xi,t_{\mathrm{F}},t)]\,\mathrm{d}\Gamma(\boldsymbol{x})\,\mathrm{d}t, \end{aligned} \tag{7}$$

where t is the time at which the responses are calculated, whereas t_0 and t_{F} are the initial and final time points and θ_0 is the initial temperature distribution. The functions $\Theta(\boldsymbol{x},\xi,t_{\mathrm{F}},t)$, $Q(\boldsymbol{x},\xi,t_{\mathrm{F}},t)$, $\overline{\Theta}_i(\boldsymbol{x},\xi,t_{\mathrm{F}},t)$, $\overline{Q}_i(\boldsymbol{x},\xi,t_{\mathrm{F}},t)$ are the fundamental solutions for two-dimentional quasistatic thermoelasticity defined elsewhere (Brebbia et al., 1984; Balas et al., 1989).

After discretizing the boundary Γ and assembling over shared nodes, Equations (6) and (7) are transformed into the following matricial form:

$$[{}_1\boldsymbol{Q}]\{{}_F\boldsymbol{\theta}\}=[{}_1\boldsymbol{\Theta}]\{{}_F\boldsymbol{q}\}+\sum_{f=1}^{F-1}\left([{}_{F+1-f}\boldsymbol{\Theta}]\{{}_f\boldsymbol{q}\}-[{}_{F+1-f}\boldsymbol{Q}]\{{}_f\boldsymbol{\theta}\}\right), \tag{8}$$

$$[\boldsymbol{T}]\{{}_F\boldsymbol{u}\}=[\boldsymbol{U}]\{{}_F\boldsymbol{t}\}+\{{}_F\boldsymbol{B}\}, \tag{9}$$

where F is the final time instant and ${}_f\theta$, ${}_fq$ are the nodal temperatures and heat fluxes at the time instant $f=1, F$, respectively. The vector $\{{}_F\boldsymbol{B}\}$ is defined as

$$\{{}_F\boldsymbol{B}\}=\sum_{f=1}^{F}\left([{}_{F+1-f}\overline{\boldsymbol{Q}}]\{{}_f\boldsymbol{\theta}\}-[{}_{F+1-f}\overline{\boldsymbol{\Theta}}]\{{}_f\boldsymbol{q}\}\right). \tag{10}$$

It must be mentioned at this point that in the present work, constant time interpolation is adopted (i.e. $\Delta t=t_f-t_{f-1}=\text{const}$) and thus, during the analysis only the matrixes $[{}_1\boldsymbol{Q}]$ and $[{}_1\boldsymbol{\Theta}]$ need to be computed and stored in memory for each additional time step (Brebbia et al., 1984; Raveendra and Banerjee, 1992).

3. Implementation of frictional crack contact

The whole procedure will be analytically explained for the case of a steady-state loading. The corresponding quasistatic problem, which virtually represents a sequence of stationary problems, is correspondingly resolved.

3.1. Incremental form of equations

Contact problems are in general non-linear since the extent of contact is not known in advance and because the friction phenomena at the contact area lead to the load history dependency of the boundary conditions. Therefore, these problems have to be formulated in an incremental and iterative fashion. In particular, the load, which in the present analysis is represented by the nodal temperatures and heat fluxes, and consequently by the vector $\{\boldsymbol{B}\}$, must be applied into small load steps defined as:

$$\{\Delta\boldsymbol{B}\}=[\overline{\boldsymbol{Q}}]\{\Delta\boldsymbol{\theta}\}-[\overline{\boldsymbol{\Theta}}]\{\Delta\boldsymbol{q}\}. \tag{11}$$

In line with the incremental theory, after m load increments, the following relationships can be considered:

$$u_i^m=u_i^{m-1}+\Delta u_i^m=\sum_{k=1}^{m}\Delta u_i^k \tag{12}$$

$$t_i^m=t_i^{m-1}+\Delta t_i^m=\sum_{k=1}^{m}\Delta t_i^k \tag{13}$$

$$B^m=B^{m-1}+\Delta B^m=\sum_{k=1}^{m}\Delta B^k. \tag{14}$$

According to Equation (4), the incremental boundary element formulation for two-dimensional steady-state thermoelasticity at an increment m can be written as:

$$[\boldsymbol{T}]\{\Delta\boldsymbol{u}^m\}=[\boldsymbol{U}]\{\Delta\boldsymbol{t}^m\}+\{\Delta\boldsymbol{B}^m\}, \tag{15}$$

where $\{\Delta\boldsymbol{u}^m\}$ and $\{\Delta\boldsymbol{t}^m\}$ are the vectors containing the incremental nodal displacements and tractions, respectively.

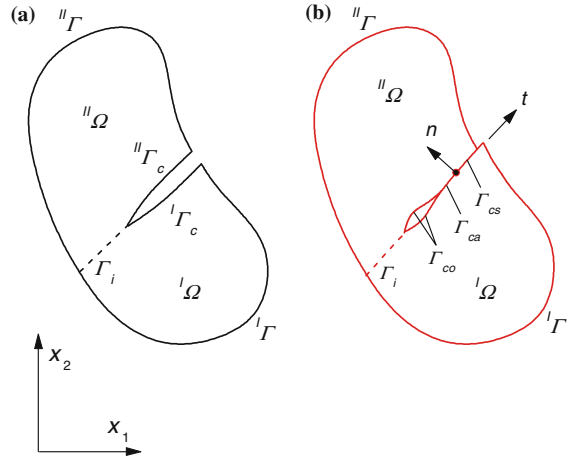

Figure 1. Cracked body subjected to thermal load: (a) open crack, and (b) partially closed crack.

The same equations are suitable for quasistatic thermoelasticity with the difference that in this case, these increments subdivide the thermal load $\{{}_F\boldsymbol{B}\}$ of a specific time point F into sub-increments $\{{}_F\Delta\boldsymbol{B}^m\}$.

3.2. Incremental contact conditions and assembly of equations

Assume a thermally loaded two-dimensional body defined in domain $\Omega(\Gamma)$, which is bounded by surface Γ. This body is fractured by an edge crack that forms the additional boundary surface $\Gamma_c = {}^{\mathrm{I}}\Gamma_c + {}^{\mathrm{II}}\Gamma_c$. The extension of this surface ahead the crack tip represents a fictitious interface Γ_i, which divides the domain of the problem into sub-domains ${}^{\mathrm{I}}\Omega$ and ${}^{\mathrm{II}}\Omega$, such that $\Omega(\Gamma) = {}^{\mathrm{I}}\Omega({}^{\mathrm{I}}\Gamma) + {}^{\mathrm{II}}\Omega({}^{\mathrm{II}}\Gamma)$ (Figure 1). This is a *tight interface*, in the sense that full continuity and compatibility are defined on it. In a general case, the crack surfaces are divided into three possible contact zones, Γ_{co}, Γ_{ca}, Γ_{cs}, which correspond to the open, adhesion and slip state, respectively. By dividing the crack surfaces ${}^{\mathrm{I}}\Gamma_c$, ${}^{\mathrm{II}}\Gamma_c$ into elements and nodes whose disposition along surfaces is identical, a number of node-pairs are created. The contact conditions, expressed in an average local coordinate system (n, t), between two nodes of a node-pair, being in one of those contact states at a load increment m are as follows:

$$\text{Open state } (\Gamma_{\mathrm{co}}):\ {}^{\mathrm{I}}t_t^m = 0;\ {}^{\mathrm{I}}t_n^m = 0;\ {}^{\mathrm{I}}t_t^m = -{}^{\mathrm{II}}t_t^m;\ {}^{\mathrm{I}}t_n^m = -{}^{\mathrm{II}}t_n^m, \tag{16}$$

$$\text{Adhesion state } (\Gamma_{\mathrm{ca}}):\ {}^{\mathrm{I}}u_t^m = {}^{\mathrm{II}}u_t^m;\ {}^{\mathrm{I}}u_n^m = {}^{\mathrm{II}}u_n^m;\ {}^{\mathrm{I}}t_t^m = -{}^{\mathrm{II}}t_t^m;\ {}^{\mathrm{I}}t_n^m = -{}^{\mathrm{II}}t_n^m, \tag{17}$$

$$\text{Slip state } (\Gamma_{\mathrm{cs}}):\ {}^{\mathrm{I}}u_n^m = {}^{\mathrm{II}}u_n^m;\ {}^{\mathrm{I}}t_t^m = \pm\mu\,{}^{\mathrm{I}}t_n^m;\ {}^{\mathrm{I}}t_t^m = -{}^{\mathrm{II}}t_t^m;\ {}^{\mathrm{I}}t_n^m = -{}^{\mathrm{II}}t_n^m. \tag{18}$$

These contact conditions express the total equilibrium and compatibility conditions. These must be always verified, but necessary for them to be rewritten in incremental form, to agree with the loading procedure. This is accomplished by substituting Equations (12) and (13) into equations (16)–(18). The following incremental contact conditions are then produced (Man et al., 1993):

$$\begin{aligned}\text{Open state } (\Gamma_{\mathrm{co}}):\ & {}^{\mathrm{I}}\Delta t_t^m = -{}^{\mathrm{I}}t_t^{m-1};\ {}^{\mathrm{I}}\Delta t_n^m = -{}^{\mathrm{I}}t_n^{m-1};\\ & {}^{\mathrm{I}}\Delta t_t^m = -{}^{\mathrm{II}}\Delta t_t^m;\ {}^{\mathrm{I}}\Delta t_n^m = -{}^{\mathrm{II}}\Delta t_n^m,\end{aligned} \tag{19}$$

$$\text{Adhesion state } (\Gamma_{ca}):\ {}^{\mathrm{I}}\Delta u_t^m = {}^{\mathrm{II}}\Delta u_t^m - {}^{\mathrm{I}}u_t^{m-1} + {}^{\mathrm{II}}u_t^{m-1};\quad {}^{\mathrm{I}}\Delta u_n^m = {}^{\mathrm{II}}\Delta u_n^m - {}^{\mathrm{I}}u_n^{m-1} + {}^{\mathrm{II}}u_n^{m-1};\quad {}^{\mathrm{I}}\Delta t_t^m = -{}^{\mathrm{II}}\Delta t_t^m;\ {}^{\mathrm{I}}\Delta t_n^m = -{}^{\mathrm{II}}\Delta t_n^m, \tag{20}$$

$$\text{Slip state } (\Gamma_{cs}):\ {}^{\mathrm{I}}\Delta u_n^m = {}^{\mathrm{II}}\Delta u_n^m - {}^{\mathrm{I}}u_n^{m-1} + {}^{\mathrm{II}}u_n^{m-1};\quad {}^{\mathrm{I}}\Delta t_t^m = \pm\mu\,{}^{\mathrm{I}}\Delta t_n^m - {}^{\mathrm{I}}t_t^{m-1} \pm \mu\,{}^{\mathrm{I}}t_n^{m-1};\quad {}^{\mathrm{I}}\Delta t_t^m = -{}^{\mathrm{II}}\Delta t_t^m;\ {}^{\mathrm{I}}\Delta t_n^m = -{}^{\mathrm{II}}\Delta t_n^m. \tag{21}$$

As can be seen, the above equations assume that slip occurs under Coulomb friction conditions with a single coefficient of friction μ. Evidently, the following incremental conditions hold on the interface Γ_i:

$$\text{Interface } (\Gamma_i):\ {}^{\mathrm{I}}\Delta u_t^m = {}^{\mathrm{II}}\Delta u_t^m;\ {}^{\mathrm{I}}\Delta u_n^m = {}^{\mathrm{II}}\Delta u_n^m;\ {}^{\mathrm{I}}\Delta t_t^m = -{}^{\mathrm{II}}\Delta t_t^m;\ {}^{\mathrm{I}}\Delta t_n^m = -{}^{\mathrm{II}}\Delta t_n^m. \tag{22}$$

Afterwards Equation (15) is applied in both sub-domains. The two resulting equations are then assembled according to all the previous mentioned incremental conditions into the following form:

$$\begin{bmatrix} {}^{\mathrm{I}}\boldsymbol{T} & \mathbf{0} & {}^{\mathrm{I}}\boldsymbol{T}_i & {}^{\mathrm{I}}\boldsymbol{T}_{\mathrm{a}} & {}^{\mathrm{I}}\boldsymbol{T}_{t,\mathrm{s}} & {}^{\mathrm{I}}\boldsymbol{T}_{n,\mathrm{s}} & \mathbf{0} & {}^{\mathrm{I}}\boldsymbol{T}_{\mathrm{o}} & \mathbf{0} \\ \mathbf{0} & {}^{\mathrm{II}}\boldsymbol{T} & {}^{\mathrm{II}}\boldsymbol{T}_i & {}^{\mathrm{II}}\boldsymbol{T}_{\mathrm{a}} & \mathbf{0} & {}^{\mathrm{II}}\boldsymbol{T}_{n,\mathrm{s}} & {}^{\mathrm{II}}\boldsymbol{T}_{t,\mathrm{s}} & \mathbf{0} & {}^{\mathrm{II}}\boldsymbol{T}_{\mathrm{o}} \end{bmatrix} \begin{Bmatrix} {}^{\mathrm{I}}\Delta\boldsymbol{u}^m \\ {}^{\mathrm{II}}\Delta\boldsymbol{u}^m \\ {}^{\mathrm{I}}\Delta\boldsymbol{u}_i^m \\ {}^{\mathrm{I}}\Delta\boldsymbol{u}_{\mathrm{a}}^m \\ {}^{\mathrm{I}}\Delta\boldsymbol{u}_{t,\mathrm{s}}^m \\ {}^{\mathrm{I}}\Delta\boldsymbol{u}_{n,\mathrm{s}}^m \\ {}^{\mathrm{II}}\Delta\boldsymbol{u}_{t,\mathrm{s}}^m \\ {}^{\mathrm{I}}\Delta\boldsymbol{u}_{\mathrm{o}}^m \\ {}^{\mathrm{II}}\Delta\boldsymbol{u}_{\mathrm{o}}^m \end{Bmatrix}$$

$$= \begin{bmatrix} {}^{\mathrm{I}}\boldsymbol{U} & \mathbf{0} & {}^{\mathrm{I}}\boldsymbol{U}_i & {}^{\mathrm{I}}\boldsymbol{U}_{\mathrm{a}} & {}^{\mathrm{I}}\boldsymbol{U}_{n,\mathrm{s}} \pm \mu\,{}^{\mathrm{I}}\boldsymbol{U}_{t,\mathrm{s}} & {}^{\mathrm{I}}\boldsymbol{U}_{\mathrm{o}} & \mathbf{0} \\ \mathbf{0} & {}^{\mathrm{II}}\boldsymbol{U} & -{}^{\mathrm{II}}\boldsymbol{U}_i & -{}^{\mathrm{I}}\boldsymbol{U}_{\mathrm{a}} & -({}^{\mathrm{II}}\boldsymbol{U}_{n,\mathrm{s}} \pm \mu\,{}^{\mathrm{II}}\boldsymbol{U}_{t,\mathrm{s}}) & \mathbf{0} & {}^{\mathrm{II}}\boldsymbol{U}_{\mathrm{o}} \end{bmatrix} \begin{Bmatrix} {}^{\mathrm{I}}\Delta\boldsymbol{t}^m \\ {}^{\mathrm{II}}\Delta\boldsymbol{t}^m \\ {}^{\mathrm{I}}\Delta\boldsymbol{t}_i^m \\ {}^{\mathrm{I}}\Delta\boldsymbol{t}_{\mathrm{a}}^m \\ {}^{\mathrm{I}}\Delta\boldsymbol{t}_{n,\mathrm{s}}^m \\ -{}^{\mathrm{I}}\boldsymbol{t}_{\mathrm{o}}^{m-1} \\ {}^{\mathrm{I}}\boldsymbol{t}_{\mathrm{o}}^{m-1} \end{Bmatrix}$$

$$- \begin{bmatrix} \mathbf{0} & \mathbf{0} \\ {}^{\mathrm{II}}\boldsymbol{T}_{\mathrm{a}} & {}^{\mathrm{II}}\boldsymbol{T}_{n,\mathrm{s}} \end{bmatrix} \begin{Bmatrix} {}^{\mathrm{I}}\boldsymbol{u}_{\mathrm{a}}^{m-1} - {}^{\mathrm{II}}\boldsymbol{u}_{\mathrm{a}}^{m-1} \\ {}^{\mathrm{I}}\boldsymbol{u}_{n,\mathrm{s}}^{m-1} - {}^{\mathrm{II}}\boldsymbol{u}_{n,\mathrm{s}}^{m-1} \end{Bmatrix} + \begin{bmatrix} {}^{\mathrm{I}}\boldsymbol{U}_{t,\mathrm{s}} \\ -{}^{\mathrm{II}}\boldsymbol{U}_{t,\mathrm{s}} \end{bmatrix} \{-{}^{\mathrm{I}}\boldsymbol{t}_{t,\mathrm{s}}^{m-1} \pm \mu\,{}^{\mathrm{I}}\boldsymbol{t}_{n,\mathrm{s}}^{m-1}\} + \{\Delta\boldsymbol{B}^m\}. \tag{23}$$

In the above equation, the subscripts o, a and s denote the nodes being in open, adhesion and slip state, respectively. Matrixes with these subscripts are written in terms of the average local coordinate system, in which the corresponding nodes are analyzed. If vector $\{\Delta\boldsymbol{B}^m\}$ is changed into $\{{}_F\Delta\boldsymbol{B}^m\}$, then the corresponding equation for the time-dependent thermoelastic problem, at the increment m of the time point F, is obtained.

3.3. Incremental–iterative procedure

The computational simplicity of the incremental-iterative procedure depends strongly on the way that thermal contact is formulated. Many researchers – in order to resolve

the thermal crack closure phenomenon – assumed that the crack faces were insulated (Kokini and Reynolds, 1991), while others assumed perfect thermal contact between the crack faces when in frictionless mechanical contact (Martin-Moran et al., 1983). In other works (Alonso and Garrido Carcia, 1995), imperfect thermal contact conditions were assumed in order to solve general frictionless thermoelastic contact problems. In this approach, the thermal resistance at the contact zone of the solids was considered to be a known decreasing function of the contact pressure. In the present work, the first two aforementioned approaches are implemented for comparative reasons.

3.3.1. *Adiabatic crack contact*

In this approach, it is assumed that the crack faces are fully adiabatic being in mechanical contact or not. This assumption uncouples the thermal solution of the problem from the mechanical one, in the sense that during the incremental procedure the thermal part of the problem does not need to be resolved according to the new contact state because thermal conditions in the contact region are not affected.

The first step of the numerical procedure, under adiabatic thermal contact conditions, is the solution of the thermal parts of the describing equations. This is accomplished by applying Equations (3) (steady-state problem) or (8) (quasistatic problem) in both sub-domains ${}^{\mathrm{I}}\Omega$ and ${}^{\mathrm{II}}\Omega$ of the problem. In order to obtain the solution, the resulting equations are assembled according to the thermal interface conditions ${}^{\mathrm{I}}\theta = {}^{\mathrm{II}}\theta$, ${}^{\mathrm{I}}q = -{}^{\mathrm{II}}q$ and the total thermal boundary conditions that describe the problem. After separating the known from the unknown boundary values of temperature and heat flux, a final solvable system of linear algebraic equations is obtained (Brebbia et al., 1984). Hereafter, the total thermal load vector $\{\boldsymbol{B}\}$ becomes known (Equations (5) and (10) for the steady-state and time-dependent problem, respectively).

The incremental procedure requires transformation of vector $\{\boldsymbol{B}\}$ into an equivalent incremental form. Two alternatives can be followed. One method is to divide vector $\{\boldsymbol{B}\}$ into a large number of small equal increments $\{\Delta\boldsymbol{B}\}$. From a physical point of view, small load steps imply that although the loads are being applied discretely, they would be continuous in the limit. At each increment of the procedure, an iterative process is followed until the extent and the nature of the contact are entirely defined. During this process every node-pair is monitored according to the conditions described in Table 1. The new contact condition is applied to the node-pair closest to such a change and after that, Equation (23) is solved again. If the change is from open state to contact state, then the adhesion state is adjusted. In this way, the determination of the sign of a future frictional traction becomes achievable because it will act in the same direction as the previous adhesive traction. When the contact area is converged to the correct one then we proceed to the next increment. Equation (23) is constructed according to the contact status of the previous increment. After solution, the same iterative procedure is introduced to seek the equilibrium state along the contact area. The procedure is continued until the final thermal load $\{\boldsymbol{B}\}$ is reached. The total quantities for the tractions and displacements are then calculated as the sum of all increments (Equations (12) and (13)).

The division of the load can also be achieved by using the well-known scaling method (Karami, 1983). According to this method, Equation (23), which is constructed by imposing the contact conditions of the previous increment, is solved for

Table 1. Determination of contact states.

Assumption	Decision	
	Open	Contact
Open	${}^{\mathrm{II}}\Delta u_n^m - {}^{\mathrm{I}}\Delta u_n^m < {}^{\mathrm{I}}u_n^{m-1} - {}^{\mathrm{II}}u_n^{m-1}$	${}^{\mathrm{II}}\Delta u_n^m - {}^{\mathrm{I}}\Delta u_n^m {}^{\mathrm{I}}u_n^{m-1} - {}^{\mathrm{II}}u_n^{m-1}$
Contact	${}^{\mathrm{I}}t_n^{m-1} + {}^{\mathrm{I}}\Delta t_n^m 0$	${}^{\mathrm{I}}t_n^{m-1} + {}^{\mathrm{I}}\Delta t_n^m < 0$
	Adhesion	Slip
Adhesion	$\left\|{}^{\mathrm{I}}t_t^{m-1} + {}^{\mathrm{I}}\Delta t_t^m\right\| < \left\|\mu({}^{\mathrm{I}}t_n^{m-1} + {}^{\mathrm{I}}\Delta t_n^m)\right\|$	$\left\|{}^{\mathrm{I}}t_t^{m-1} + {}^{\mathrm{I}}\Delta t_t^m\right\| \left\|\mu({}^{\mathrm{I}}t_n^{m-1} + {}^{\mathrm{I}}\Delta t_n^m)\right\|$
Slip	$({}^{\mathrm{I}}t_t^{m-1} + {}^{\mathrm{I}}\Delta t_t^m)({}^{\mathrm{I}}\Delta u_t^m - {}^{\mathrm{II}}\Delta u_t^m) > 0$	$({}^{\mathrm{I}}t_t^{m-1} + {}^{\mathrm{I}}\Delta t_t^m)({}^{\mathrm{I}}\Delta u_t^m - {}^{\mathrm{II}}\Delta u_t^m)0$

a test thermal load increment $\{\Delta \boldsymbol{B}\}$, which usually is chosen to be a small fraction of $\{\boldsymbol{B}\}$. After obtaining the solution, this test load increment is scaled according to the contact conditions at every candidate node-pair. Assuming linearity of response, the actual amount of the thermal load increment at each step has to be established by considering the following possible changes of contact state: (1) from open to contact state, (2) from adhesion state to slip state, and vice versa. Equation (23) is reconstructed according to the new contact condition and the procedure is continued as it was previously explained.

In the case of the quasistatic thermoelastic problem, an independent incremental procedure can be carried out for every time step F and the corresponding load $\{{}_F\boldsymbol{B}\}$ is subdivided into increments $\{{}_F\Delta\boldsymbol{B}\}$ in a similar way. It has to be noted at this point, that problems of straight cracks are contact problems of the conforming type since the crack faces have the same shape in the unloaded state and therefore, the contact area is load independent. Despite this fact, the areas of adhesion and slip can be still load-dependent and thus, these problems have to be solved incrementally.

3.3.2. *Perfect thermal crack contact*

When perfect thermal crack contact is assumed, the non-linearity of the problem is increased in the sense that at each stage of the procedure, the change in the extent of mechanical contact influences the thermal boundary conditions in the crack region and consequently, the thermal solution of the problem. In order to proceed to the next stage of the procedure, the size of the thermal contact zone must first converge to the size of the mechanical contact zone. The form of the incremental-iterative procedure for a quasistatic thermoelastic problem, under perfect thermal contact conditions, is schematically explained in the flow chart of Figure 2 (the algorithm for a stationary thermoelastic problem is obtained by ignoring the time values f, F in the flow chart). It should be noted that in this case, the solution of each time point F cannot be carried out independently as it could be done in the case of adiabatic crack contact assumption. The solution now must be carried out sequentially for every time point $f = 1, F$.

4. Thermal SIFs

The previously developed formulation aims to the evaluation of fracture characteristics of partially or fully closed cracks under thermal loading. In the vicinity of the

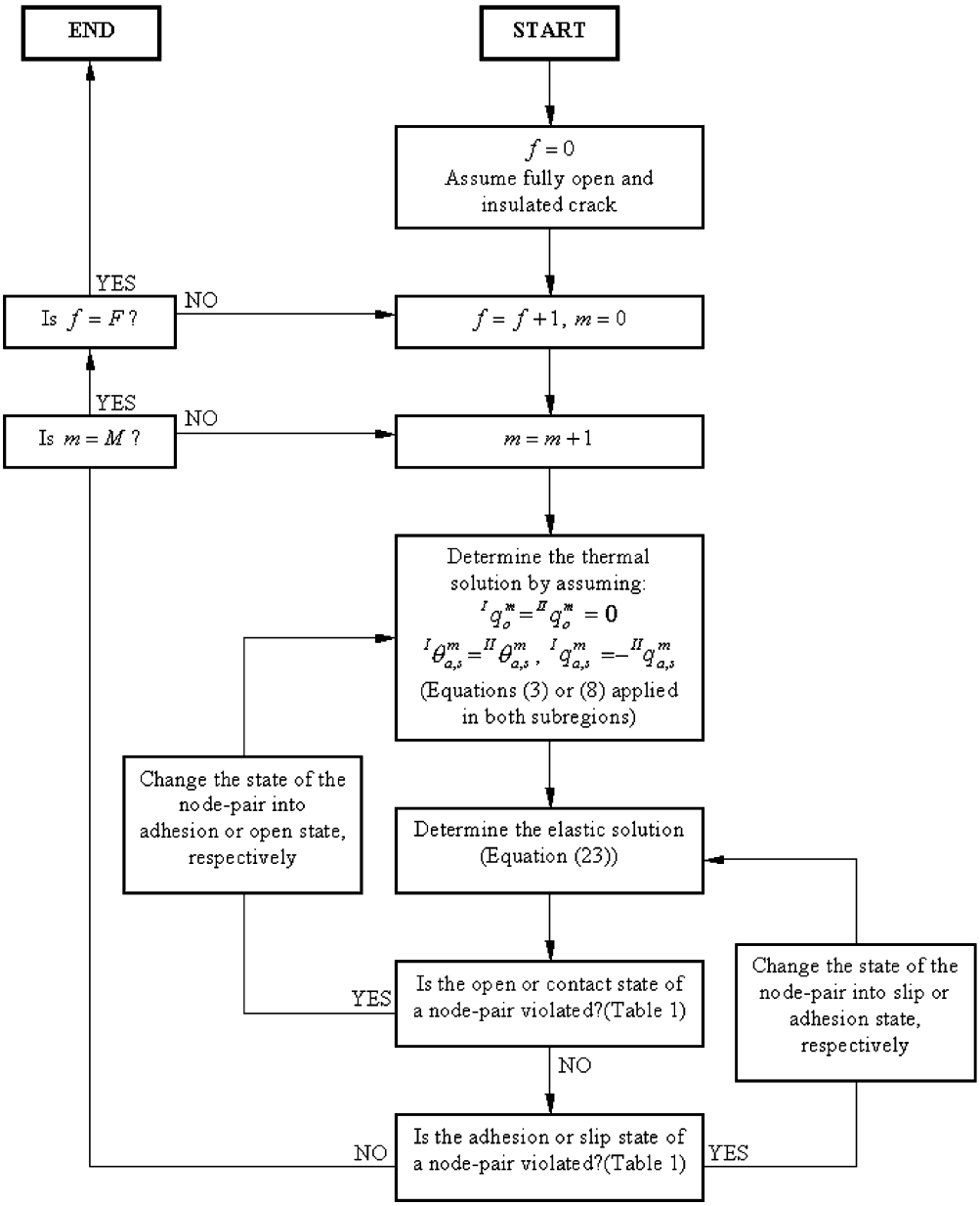

Figure 2. Incremental-iterative procedure for a quasistatic thermoelastic problem, under perfect thermal contact conditions.

tip of a thermal crack, the singularity of heat flux is characterized by the flux intensity factor (FIF) denoted as k_{T}, while the singularity of stresses is characterized by the mode-I and mode-II thermal stress intensity factors (TSIFs), denoted as k_{I} and k_{II}, respectively.

When the multi-domain technique is used, the near crack tip behavior may be included in the boundary element approach by utilizing QPEs and traction singular QPEs (TSQPEs) crack tip elements. Figure 3 illustrates the proper usage of these

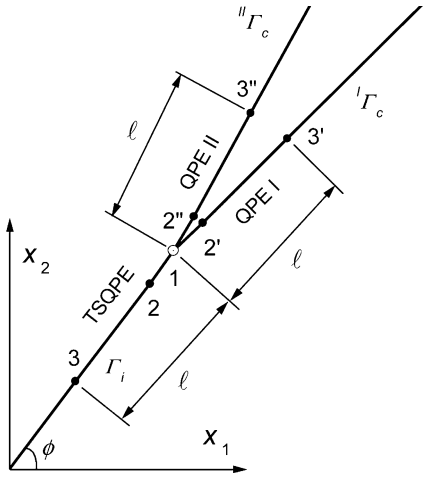

Figure 3. Configuration of crack tip elements.

elements. The QPE is described by the shape functions of a typical quadratic isoparametric element, having its middle node moved to the quarter of its length. The shape functions of TSQPE are produced by multiplying the shape functions of QPEs by the factor $2/(1+\zeta)$, where ζ is the natural coordinate over the element. These elements approximate directly the crack tip behavior of temperature and displacement fields and their gradients. Details of these derivations and the performance of the involved singular elements may be found elsewhere (Martinez and Dominguez, 1984; Katsareas and Anifantis, 1996).

The generalized traction formula is the most stable and accurate method for evaluating fracture parameters. In the case of a slant crack, this formula may be expressed in the form:

$$\boldsymbol{K} = \sqrt{2\pi\ell} \begin{bmatrix} 0 & 1 & 0 \\ 1 & 0 & 0 \\ 0 & 0 & 1 \end{bmatrix} \begin{bmatrix} \boldsymbol{T} & & 0 \\ & & 0 \\ 0 & 0 & 1 \end{bmatrix} \begin{Bmatrix} p_1 \\ p_2 \\ q_1 \end{Bmatrix}, \tag{24}$$

where

$$\boldsymbol{T} = \begin{bmatrix} \cos\phi & \sin\phi \\ -\sin\phi & \cos\phi \end{bmatrix} \tag{25}$$

is the rotation matrix, ϕ is the crack orientation angle, ℓ is the crack element length and vector $\boldsymbol{K} = \{k_{\mathrm{I}} \quad k_{\mathrm{II}} \quad k_{\mathrm{T}}\}^T$ represents the field intensification. Equation (24) represents a generalized traction formula, which permits evaluation of TSIFs and FIF. In order to evaluate these characteristics through Equation (24), only the traction and heat flux values at crack tip node 1 which belongs to TSQPE, are required. Due to the position of this node as independent on the element length ℓ, the traction formula is expected to give less sensitive results to ℓ.

5. Numerical results and discussion

The proposed BEM numerical procedure was developed in order to solve frictional crack contact problems, assuming adiabatic or perfectly conductive crack faces,

initially subjected to traction free conditions. At each increment of the procedure, a boundary element analysis is performed, TSIFs are evaluated and contact conditions are updated to confirm with contact criteria. In order to elucidate the performance of the proposed numerical procedure, computational results are presented, concerning mainly the calculation of TSIFs when frictional crack contact takes place, under steady-state and transient heating conditions. Two representative test problems are selected. The first example involves an edge cracked strip subjected to steady-state heat conduction, whereas, the second example involves a rapidly heated body containing a slant edge crack.

The numerical procedure could not be verified by comparisons with experimental results due to the lack of experimental studies associated with thermoelastic frictional crack closure problems. However, the validity accuracy of the procedure is generally proved through comparisons with existing analytical solutions involving crack closure induced by thermal shock (Nied, 1987).

5.1. Frictional crack contact under steady-state conditions

Figure 4 depicts the first problem of interest. An edge cracked strip of width W is subjected to one-dimensional steady-state heat transfer. Plane strain conditions are assumed. The upper surface is hot at a temperature T_h while the lower surface is cool at a temperature T_c, such that $T_h = -T_c$. In order to determine a far field solution, a segment of total length $2L = 2(2W)$, having its vertical sides insulated and horizontally constrained, is analyzed. A relatively coarse mesh of 28 elements per sub-domain is used. Crack surface is discretized into seven elements per sub-domain. In all cases, QPEs and TSQPEs are used as crack tip elements along the crack faces and the interface, respectively. Numerical tests have shown that if more dense mesh refinements are utilized, then the resulting difference on TSIFs values is less than 1%. TSIFs were extracted for a crack of depth $\alpha/W = 0.8$ and a crack tip element of length $\ell/\alpha = 0.02$, via equation (24). In all cases, a partial closure of the crack was observed. Figures 5 and 6 illustrate the variation of opening and shearing fracture modes of steady-state TSIFs, respectively, vs. the crack orientation angle ϕ and several coefficients of friction. The results correspond to the adiabatic contact assumption as well as to the perfect thermal contact assumption. TSIFs were normalized according to the following relationships:

$$K_I = \frac{(1-\nu)k_I}{E\alpha_t(T_h - T_c)\sqrt{W}}; \quad K_{II} = \frac{(1-\nu)k_{II}}{E\alpha_t(T_h - T_c)\sqrt{W}}, \tag{26}$$

where E, ν, α_t are the modulus of elasticity, the Poisson's ratio and the coefficient of thermal expansion, respectively. The magnitude of the coefficient of friction between crack surfaces seems to have minor influence on the opening mode TSIF while it significantly affects the shearing mode TSIF. The effect of friction on the opening TSIF becomes more distinct for greater angles ϕ.

The use of perfect thermal contact conditions along the crack had no effect on the closure lengths for the whole range of angles. For all cases, the same open crack areas near the crack tip were observed. As it can be seen from the figures, the flow between the crack faces along the contact zone has as – a result – a small increase in the magnitude of TSIFs II especially for higher angles while TSIFs I was negligibly influenced.

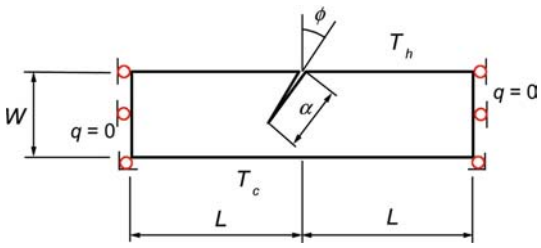

Figure 4. Geometry of edge cracked strip subjected to steady-state heat transfer.

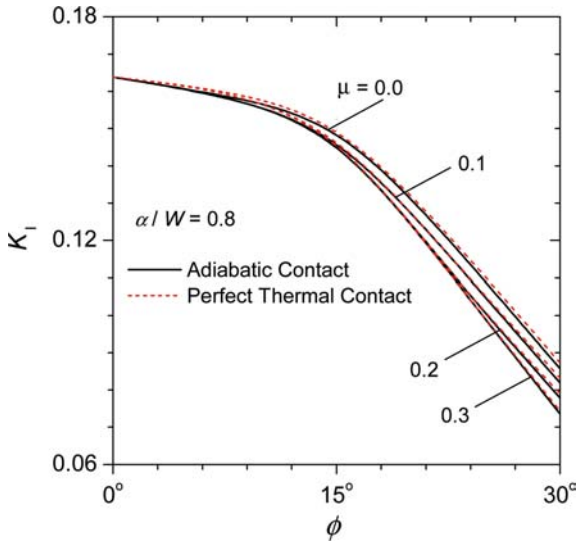

Figure 5. Effect of friction on opening fracture mode TSIF.

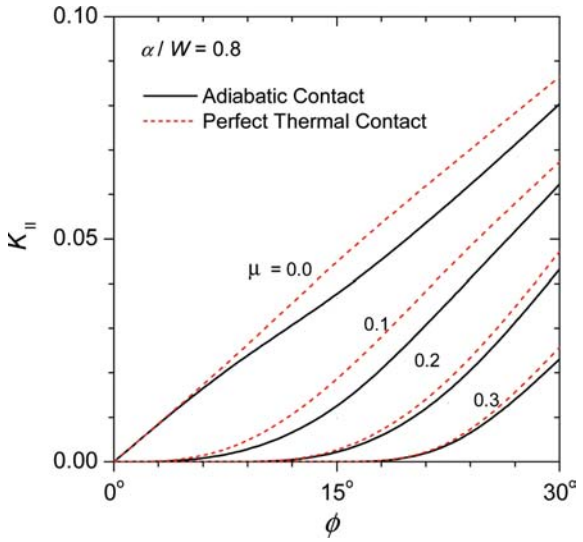

Figure 6. Effect of friction on shearing fracture mode TSIF.

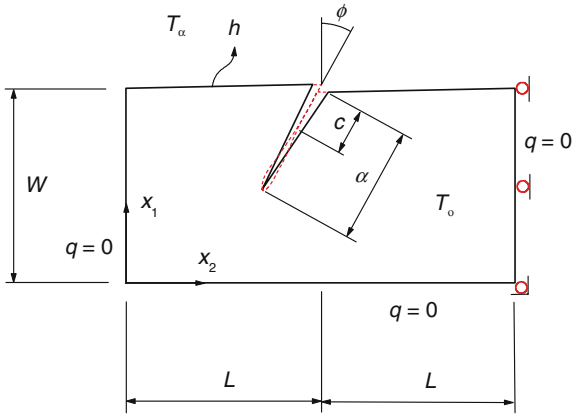

Figure 7. Geometry of edge cracked body subjected to transient convective heating.

5.2. Frictional crack contact under sudden heating

Figure 7 depicts a two-dimensional body of width W and total length of $2L = 2W$, at an initial temperature T_0. The body contains an edge crack of depth α and slope ϕ. Plane strain conditions are once more assumed. At time $t_0 = 0$ the cracked surface of the body is suddenly subjected to convective heating with the heat transfer coefficient given by h, and the ambient temperature maintained at T_α, such that $T_\alpha > T_0$. The appropriate far field boundary conditions are imposed (Figure 7). The crack has a depth of $\alpha/W = 0.1$. A coarse mesh of 24 elements per sub-domain is used while each crack face is discretized into seven elements. In all cases, QPEs and TSQPEs are used as crack tip elements along the crack faces and the interface, respectively. The time histories of mode-I and mode-II thermal shock SIFs (TSSIFs) are normalized according to the following equations:

$$K_{\mathrm{I}}(\tau) = \frac{(1-\nu)k_{\mathrm{I}}(t)}{E\alpha_t(T_\alpha - T_0)\sqrt{\pi\alpha}}; \qquad K_{\mathrm{II}}(\tau) = \frac{(1-\nu)k_{\mathrm{II}}(t)}{E\alpha_t}(T_\alpha - T_0)\sqrt{\pi}\alpha, \tag{27}$$

where τ is the normalized time $\tau = Dt/W^2$ (Fourier number) and D is the diffusivity of the body. The numerical results that are presented in the following correspond to different Biot numbers. Biot number is a non-dimensional quantity equal to $\mathrm{Bi} = hW/k$, where k is the thermal conductivity of the body. When the upper surface of the body is subjected to sudden convective heating, obviously there is $\mathrm{Bi} = \infty$.

Firstly, it is assumed that $\phi = 0^\circ$ and that $u_1(x_1 = 0, x_2 = 0) = 0$, $u_2(x_1 = 0, x_2 = 0) = 0$, $u_1(x_1 = 0, x_2 = 2L) = 0$ are the constrains of the cracked body. These specific constraints are selected in order to permit a symmetric deformation of the body towards the axis $x_2 = L$. This test case is selected in order to examine the validity of the developed numerical procedure by comparison with the analytical solutions provided by Nied (1987). These analytical solutions correspond to the thermal fracture problem of an infinite ($2L = \infty$) edge cracked body subjected to uniform surface heating exactly as the thermal boundary conditions of Figure 7 imply. The heating of the upper surface of the body produces compressive thermal stresses which cause the closure of the crack over a certain contact length $c = c(t)$. However, the area near the crack tip is located in the tensile stress region and thus it remains open for an initial

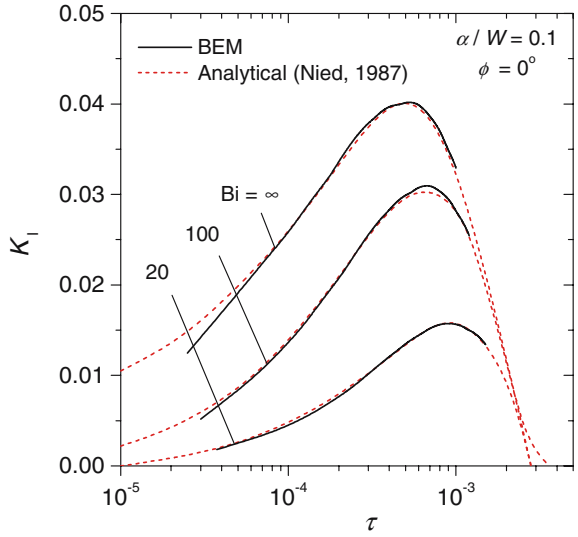

Figure 8. Time history of opening fracture mode TSSIF for the test case $\phi = 0^\circ$.

period of time. The contact length constantly increases and finally full crack closure is observed. Figure 8 presents the computed time histories of normalized mode-I TSSIF for three different Biot numbers. Because of the symmetry of the problem, mode-II TSSIF does not exist. Figure 9 depicts the normalized contact length c/a vs. normalized time, for $\mathrm{Bi} = \infty$. Due to the symmetry of the problem all the computed values showed independency on the coefficient of friction. For the same reason, identical results are obtained if we assume either that the crack is insulated or that perfect thermal contact occurs along the contact zone. It should be noted, that the problem was additionally solved for the cases $2L = 2(2W)$ and $2L = 4(2W)$. It was found that the percentage differences in mode-I TSSIF peak values which appeared at the same time points, were less than 2% in comparison with the case $2L = 2W$. This indicates that the aspect ratio $2L = 2W$ is sufficient for the time-dependent solution to converge to the solution of the infinite problem ($2L = \infty$).

Secondly, it is assumed that $\phi = 30^\circ$ and that $u_1(x_1 = 0, x_2 = 2L) = 0$, $u_2(0 \leqslant x_1 \leqslant W, x_2 = 2L) = 0$ are the constraints of the cracked body (Figure 7). Figures 10 and 11 illustrate the time history of mode-I and mode-II TSSIFs in normalized form, respectively. The results that are included in these two figures correspond to the adiabatic crack contact assumption as well as the perfect thermal crack contact assumption. As it can be seen, the peak values depend on the friction conditions imposed on crack surfaces. Friction increases the peak values of the opening fracture mode TSSIF and decreases those of shearing fracture mode TSSIF. When great coefficients of friction are utilized, then the shearing mode TSSIF tends to zero while the opening mode TSSIF gets very high values. Furthermore, it is observed that the perfect thermal contact approach leads to slightly higher peak values of both mode-I and mode-II TSSIFs. Figure 12 illustrates the normalized contact length c/a vs. normalized time, for $\mathrm{Bi} = \infty$ and $\mu = 0$. The contact length showed independency from the coefficient of friction of the crack surfaces. Figures 13 and 14 illustrate the peak values K_{Ip}, K_{IIp} of opening and shearing fracture mode TSSIFs, respectively, with respect to Biot

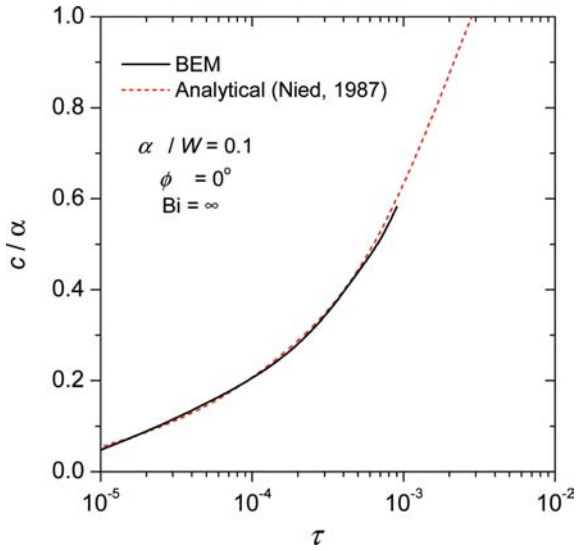

Figure 9. Variation of contact length for the test case $\phi = 0^{\circ}$.

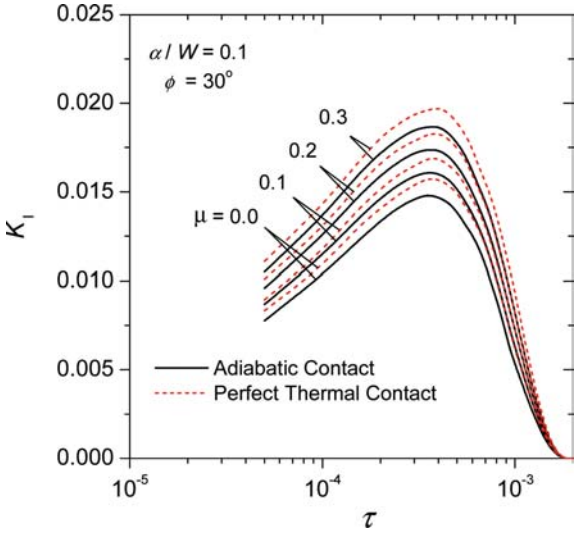

Figure 10. Time history of opening fracture mode TSSIF.

number for various coefficients of friction. These results show that when the friction coefficient increases, the opening fracture mode TSSIF increases while the shearing mode TSIF decreases. Although K_{Ip} values appear earlier than the corresponding K_{IIp} values, the time shift between them is nearly constant and independent on the friction coefficient. Finally, Figure 15 shows the delay of peak values of TSSIFs vs. Biot number, for $\mu = 0$. Obviously, for high Biot numbers we have rapid appearances of K_{Ip}, K_{IIp}. Once more, the coefficient of friction had a negligible influence on the values τ_{p} of both modes for a certain Biot number.

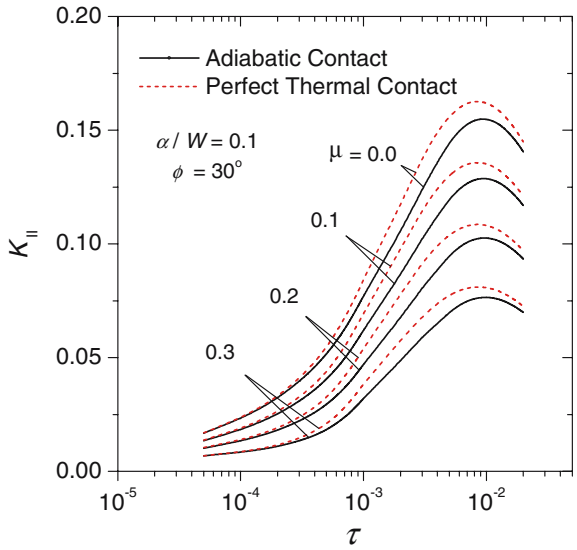

Figure 11. Time history of shearing fracture mode TSSIF.

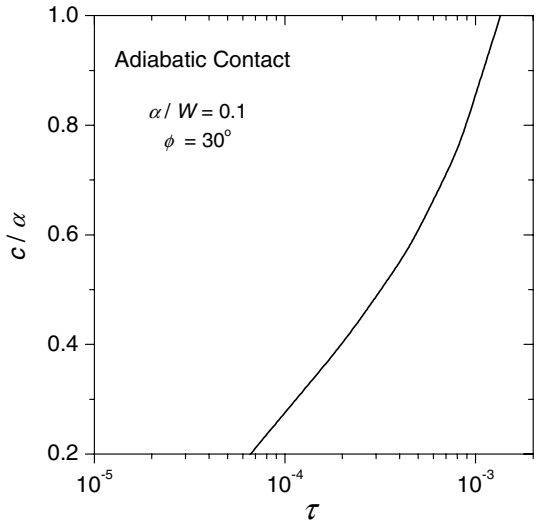

Figure 12. Variation of contact length.

6. Conclusions

A numerical procedure based on the BEM capable of solving problems that involve frictional crack surface interference provoked by stationary and transient thermal loading, is presented in this paper. The multi-domain formulation has been adopted and quadratic isoparametric representation of geometries has been employed, for the analysis of two dimensional crack problems. Crack faces have been modeled as boundaries of independent sub-domains of the body, and field singularities have been incorporated through the use of appropriate crack-tip elements. An iterative-incremental process has been developed in order to deal with the non-linearity of the

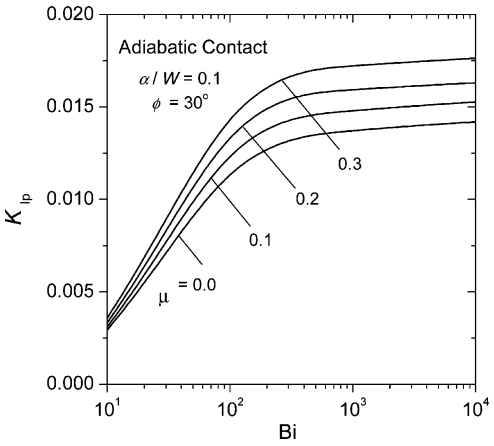

Figure 13. Variation of peak values of opening fracture mode TSSIF vs. Biot number.

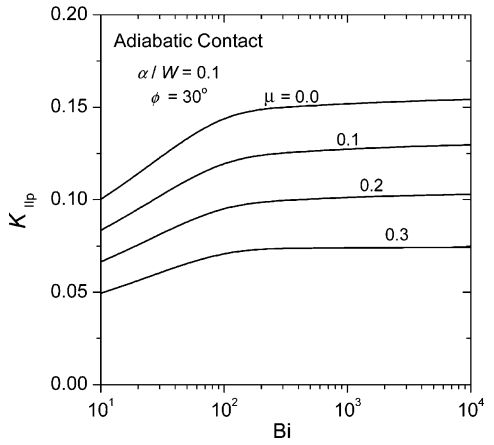

Figure 14. Variation of peak values of shearing fracture mode TSSIF vs. Biot number.

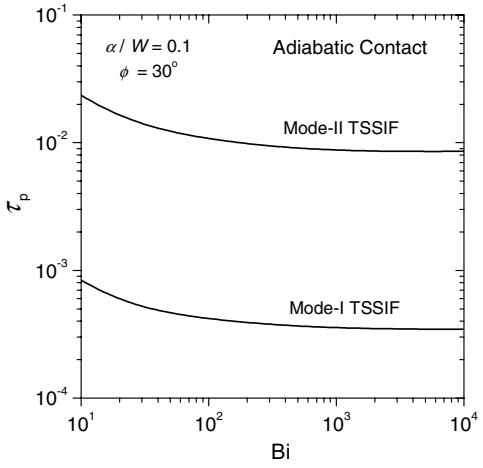

Figure 15. Delay of peak values of TSSIFs vs. Biot number for the case.

crack surface interference. Along the contact areas, proper mechanical and thermal conditions have been imposed.

Various results involving TSIFs and contact length have been presented. It has been proven that even for coarse mesh refinement along crack faces, the method converges rapidly and yields accurate results in comparison with analytical solutions. The effect of crack closure on TSIFs has been extensively investigated under various thermal boundary and contact conditions, crack orientations and coefficients of friction. It has been confirmed that the contact of the crack faces has a great impact on the fracture parameters and thus, its proper modeling is considered significant. It has also been proven, for the test problems considered here, that the utilization of perfect thermal contact conditions – instead of adiabatic contact conditions along the crack closure zone – does not lead to significantly different estimation of TSIFs. The proposed method has been proven to be a potent numerical tool in predicting frictional fracture interference characteristics even in cases of severe thermal shocks. Having the proposed method as a basis, the effect of the imperfect thermal contact assumption on frictional crack closure problems could be analyzed in a future work.

References

Alonso, P. and Garrido Garcia, J.A. (1995). BEM applied to 2D thermoelastic contact problems including conduction and forced convection in interstitial zones. *Engineering Analysis with Boundary Elements* **15**, 249–259.

Anifantis, N.K. (2001). Crack surface interference: a finite element analysis. *Engineering Fracture Mechanics* **68**, 1403–1415.

Balas, J., Sladek, J. and Sladek, V. (1989). *Stress Analysis by Boundary Element Methods*. Elsevier, Amsterdam.

Brebbia, C.A., Telles, J.C.F. and Wrobel, L.C. (1984). *Boundary Element Techniques*. Springer, Berlin.

Karami, G. (1983). A boundary element method for two-dimensional elastic contact problems. PhD. thesis. Mechanical Engineering Department, Imperial College of Science and Technology, University of London.

Karami, G. and Fenner, R.T. (1986). Analysis of mixed mode fracture and crack closure using the boundary integral equation method. *International Journal of Fracture* **30**, 13–29.

Katsareas, D.E. and Anifantis, N.K. (1995). On the computation of mode I and mode II thermal shock stress intensity factors using a boundary-only element method. *International Journal for Numerical Methods in Engineering* **38**, 4157–4169.

Katsareas, D.E. and Anifantis, N.K. (1996). Performance of quarter-point boundary elements in analyzing thermally stressed kinked and curved cracks. *Computer Methods in Applied Mechanics and Engineering* **137**, 153–165.

Kokini, K. and Reynolds, R.R. (1991). Transient heating vs. cooling of interfacial cracks in ceramic-to-metal bonds. *Engineering Fracture Mechanics* **38**, 371–383.

Liu, S.B. and Tan, C.L. (1992). Two-dimensional boundary element contact mechanics analysis of angled crack problems. *Engineering Fracture Mechanics* **42**, 273–288.

Man, K.W., Aliabadi, M.H. and Rooke, D.P. (1993). Bem frictional contact analysis: Load incremental technique. *Computers and Structures* **47**, 893–905.

Martin-Moran, C.J., Barber, J.R. and Comninou, M. (1983). The penny-shaped interface crack with heat flow. Part1: Perfect contact. *ASME Journal of Applied Mechanics* **50**, 29–36.

Martinez, J. and Dominguez, J. (1984). On the use of quarter-point boundary elements for stress intensity factor computations. *International Journal for Numerical Methods in Engineering* **20**, 1941–1950.

McClung, R.C.and Sehitoglou, H. (1989). On the finite element analysis of fatigue crack closure-1. Basic modeling issues. *Engineering Fracture Mechanics* **33**, 237–252.

Nied, H.F. (1983). Thermal shock fracture in an edge-cracked plate. *Journal of Thermal Stresses* **6**, 217–226.

Nied, H.F. (1987). Thermal shock in an edge-cracked plate subjected to uniform surface heating. *Engineering Fracture Mechanics* **26**, 239–246.

Raveendra, S.T. and Banerjee, P.K. (1992). Boundary element analysis of cracks in thermally stressed planar structures. *International Journal of Solids and Structures* **29**, 2301–2317.

Rizk, A. and El-Fattah, A. (1993). A cracked plate under transient thermal stresses due to surface heating. *Engineering Fracture Mechanics* **45**, 687–696.

Selvadurai, A.P.S. and Au, M.C. (1988). Crack with frictional interfaces: a boundary element approach, Proceedings of 10th Conference in *Boundary Element Methods in Engineering*, (Edited by Brebbia, C.A.), Vol. 3. CMP, Southampton and Springer-Verlag, Berlin, pp.211–230.

Zang, W.L. and Gudmundson, P. (1990). Contact problems of kinked cracks modeled by a boundary integral equation method. *International Journal for Numerical Methods in Engineering* **29**, 847–860.